

Electronic supplementary information

Simulated conformality of atomic layer deposition in lateral channels: the impact of the Knudsen number on the saturation profile characteristics

Christine Gonsalves,^{*a} Jorge A. Velasco,^a Jihong Yim,^a Jänis Järvilehto,^a Ville Vuorinen,^b and Riikka L. Puurunen^{*a}

^a Department of Chemical and Metallurgical Engineering, Aalto University, P.O. Box 16100, FI-00076 AALTO, Finland.

^b School of Engineering, Aalto University, P.O. Box 16100, FI-00076 AALTO, Finland.

* Corresponding authors. E-mail: christine.gonsalves@aalto.fi, riikka.puurunen@aalto.fi

† Electronic supplementary information (ESI) available.

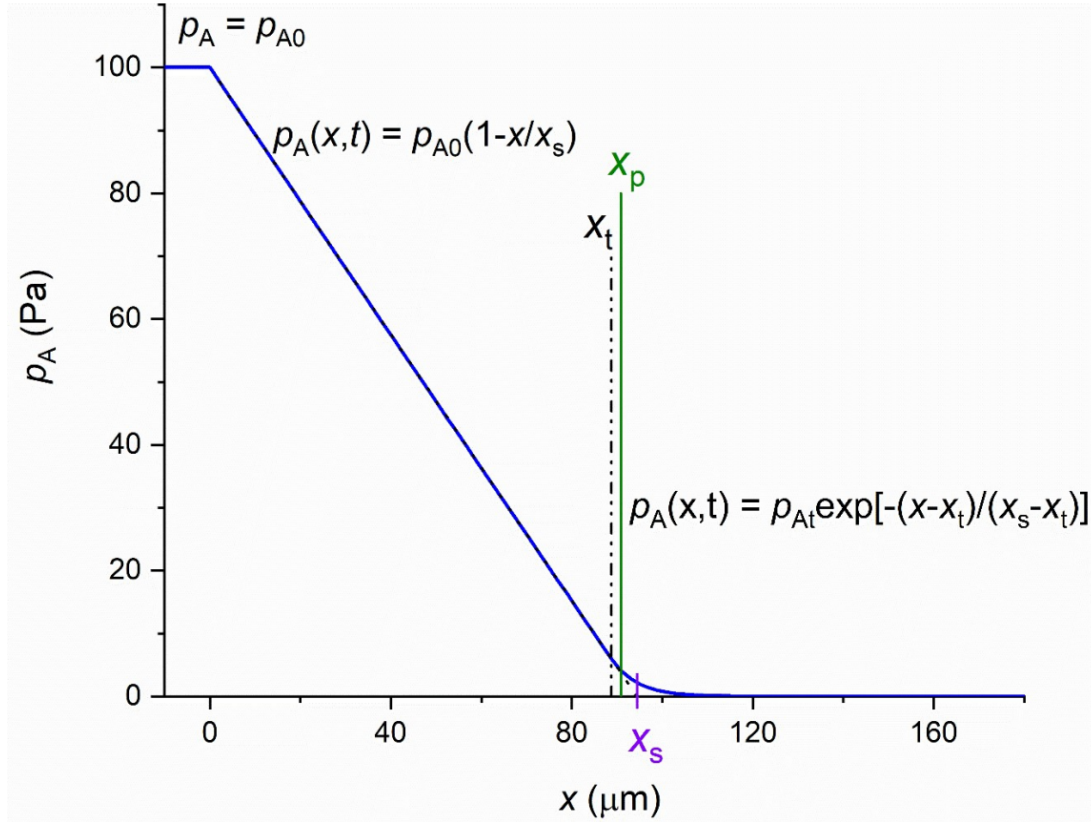


Figure S1 Partial pressure profile of reactant A p_A as function of distance x . Pressure decreases linearly before the transition point x_t is reached (Eq. 18). Linearly extrapolated pressure becomes zero at x_s . Beyond the transition point, when $x > x_t$, an approximation is used as in Eqs. 20 and 21. In this illustration, x_p is the penetration depth at half surface coverage. Reproduced from the supplementary figure (Fig. S1) of Yim *et al.*¹, Creative Commons Attribution 3.0 Unported Licence.

S1 Varying exposure series

S1.1 Total exposure calculation

Calculated values of the total exposure for pressures varying from 10^{-2} to 10^4 Pa with a constant exposure time of 0.1 s are in table S1. Exposure was varied within 10^{-3} to 10^3 Pa·s.

Table S1 Exposures calculated for the varying exposure series

Reactant partial pressure p_{A0} Pa	Exposure time t s	Total exposure Pa·s	Total exposure Langmuir
10^{-2}	10^{-1}	10^{-3}	7.5×10^0
10^{-1}	10^{-1}	10^{-2}	7.5×10^1
10^0	10^{-1}	10^{-1}	7.5×10^2
10^1	10^{-1}	10^0	7.5×10^3
10^2	10^{-1}	10^1	7.5×10^4
10^3	10^{-1}	10^2	7.5×10^5
10^4	10^{-1}	10^3	7.5×10^3

S1.2 Estimation of the total exposure to saturate the surface at LHAR channel entrance

Total exposure expected to saturate the surface at the entrance of the LHAR structure was calculated from the Gordon et al. model² (Eq. 7: $Pt = S\sqrt{2\pi mk_B T}$; S corresponds to q in this work). Dividing the result at 250°C with the sticking coefficient c of 0.01 gave 0.029 Pa·s (~ 220 L) as the expected total exposure for saturation.

Simulation results presented in the main article (Fig. 3a-h) show that for the cases with p_{A0} 10^{-2} , 10^{-1} , and 10^0 Pa, complete surface coverage was not yet seen at the entrance of the LHAR channel. Thus, the corresponding total exposures (10^{-3} , 10^{-2} , 10^{-1} Pa·s, ~ 7.5 , 75 , 750 L respectively) were insufficient to saturate the surface. The case with p_{A0} of 10^0 Pa had total exposure of 10^{-1} Pa·s (~ 750 L), which is higher than the exposure expected to be required for full surface coverage at the channel entrance calculated with the Gordon et al.² method. The reason for the higher total exposure required for saturation in the simulations as compared to the calculated value remains unclear.

S2 Constant exposure series

S2.1 Total exposure calculation

Calculated values of the total exposure for pressures varying from 10^{-2} to 10^4 Pa and exposure time varying from 10^{-3} to 10^3 s are in table S2. Exposure was 10 Pa·s in all cases.

Table S2 Reactant partial pressure and exposure time calculated for the constant exposure series

Reactant partial pressure p_{A0} Pa	Exposure time t s	Total exposure Pa·s	Total exposure Langmuir
10^{-2}	10^3	10	7.5×10^4
10^{-1}	10^2	10	7.5×10^4
10^0	10^1	10	7.5×10^4
10^1	10^0	10	7.5×10^4
10^2	10^{-1}	10	7.5×10^4
10^3	10^{-2}	10	7.5×10^4
10^4	10^{-3}	10	7.5×10^4

S3 Supplementary information presented for both the constant and varying exposure series

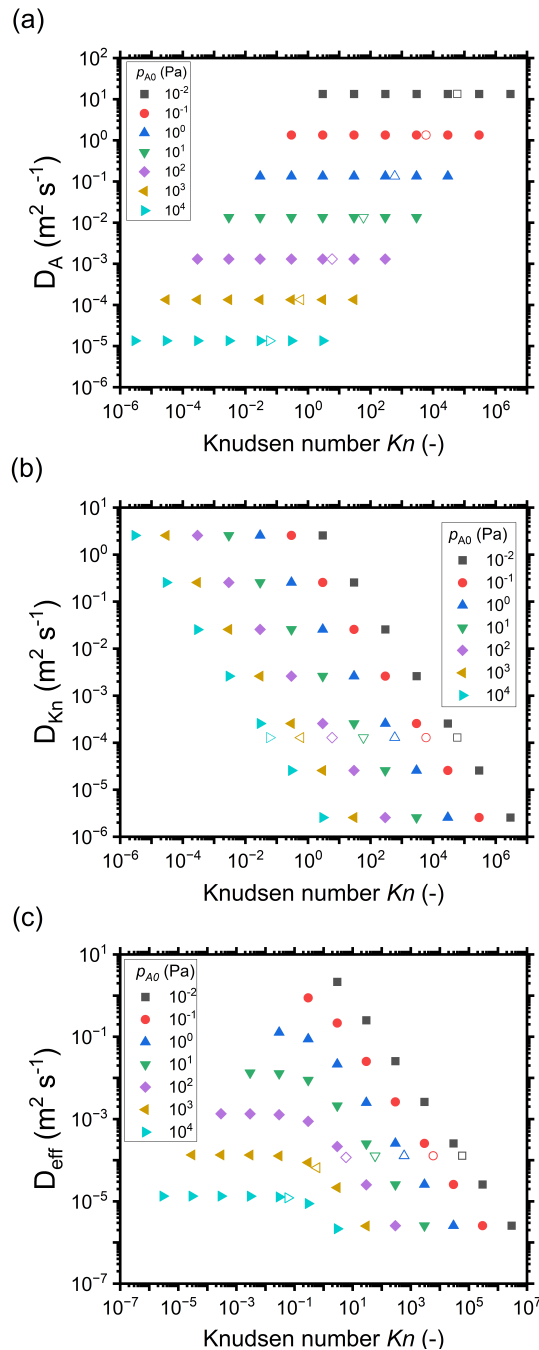


Figure S2 Diffusion coefficients ($\text{m}^2 \text{s}^{-1}$) as a function of the Kn number, for different reactant partial pressure p_{A0} : (a) molecular diffusion coefficient D_A , (b) Knudsen diffusion coefficient D_{Kn} , and (c) effective diffusion coefficient D_{eff} . Hollow symbols represent a 500 nm channel height and correspond to the PillarHallTM case.³

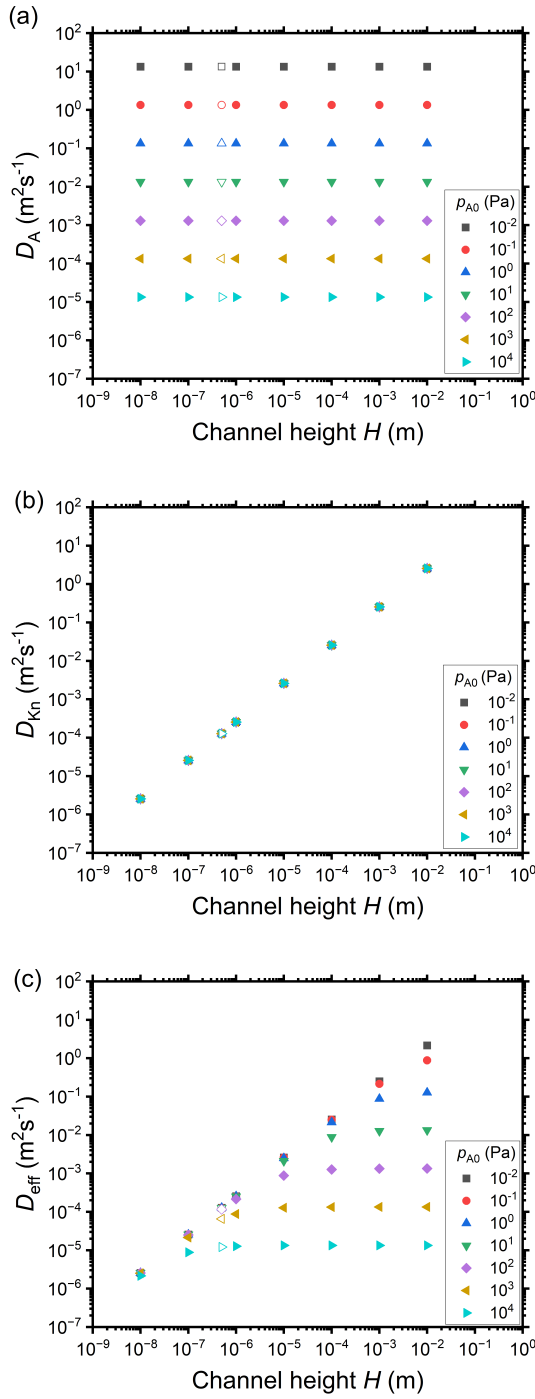
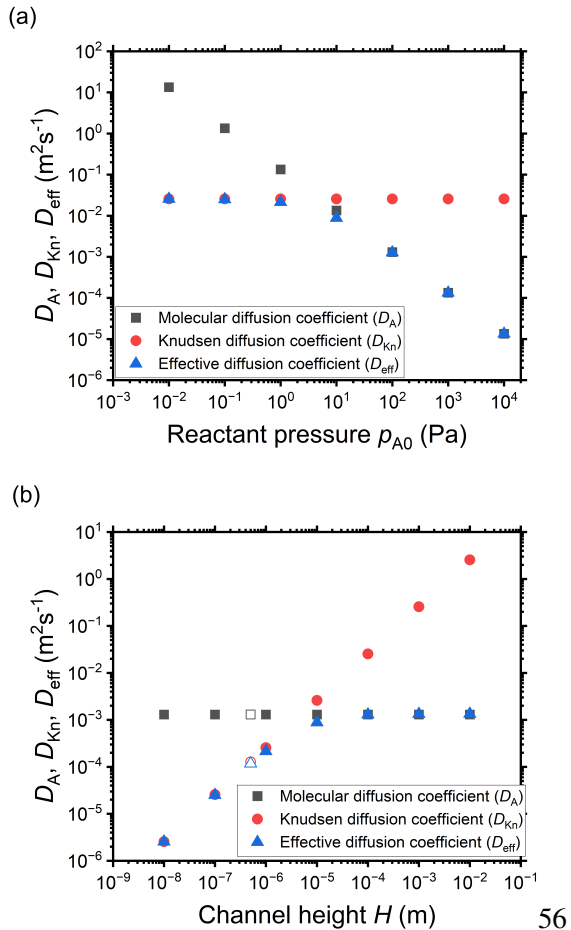


Figure S3 Diffusion coefficients ($\text{m}^2 \text{s}^{-1}$) as a function of the channel height H , for different reactant partial pressure p_{A0} : (a) molecular diffusion coefficient D_A , (b) Knudsen diffusion coefficient D_{Kn} , and (c) effective diffusion coefficient D_{eff} . Hollow symbols represent a 500 nm channel height and correspond to the PillarHallTM case.³



56

Figure S4 Diffusion coefficients ($m^2 s^{-1}$) as a function of: (a) reactant pressure p_{A0} , with a constant H of $100 \mu\text{m}$, and (b) channel height H , with a constant p_{A0} of 10^2 Pa . Hollow symbols are for the PillarHallTM case³ with a 500 nm channel height.

Table S3 Conditions corresponding to Knudsen number values for data selected from saturation profiles of Figure 7 of the main article plotted together in

Figure 9 of the main article. The selected data points are marked in bold.

Channel height H (m)	Knudsen number					
	$p_{A0} = 10^{-2}$ Pa	$p_{A0} = 10^{-1}$ Pa	$p_{A0} = 10^0$ Pa	$p_{A0} = 10^1$ Pa	$p_{A0} = 10^2$ Pa	$p_{A0} = 10^3$ Pa
10^{-8}	2.96×10^6	2.96×10^5	2.96×10^4	2.96×10^3	2.96×10^2	2.96×10^1
10^{-7}	2.96×10^5	2.96×10^4	2.96×10^3	2.96×10^2	2.96×10^1	2.96×10^0
10^{-6}	2.96×10^4	2.96×10^3	2.96×10^2	2.96×10^1	2.96×10^0	2.96×10^{-1}
10^{-5}	2.96×10^3	2.96×10^2	2.96×10^1	2.96×10^0	2.96×10^{-1}	2.96×10^{-2}
10^{-4}	2.96×10^2	2.96×10^1	2.96×10^0	2.96×10^{-1}	2.96×10^{-2}	2.96×10^{-3}
10^{-3}	2.96×10^1	2.96×10^0	2.96×10^{-1}	2.96×10^{-2}	2.96×10^{-3}	2.96×10^{-4}
10^{-2}	2.96×10^0	2.96×10^{-1}	2.96×10^{-2}	2.96×10^{-3}	2.96×10^{-4}	2.96×10^{-5}
500 nm (PillarHall™)	5.92×10^4	5.92×10^3	5.92×10^2	5.92×10^1	5.92×10^0	5.92×10^{-1}
						5.92×10^{-2}

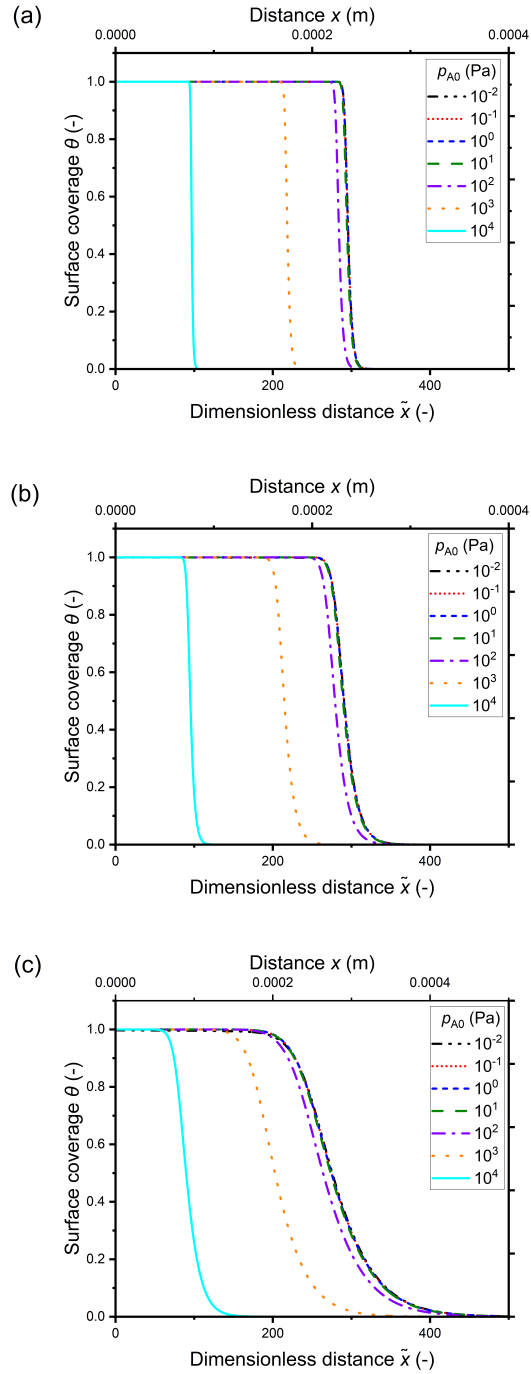


Figure S5 Saturation profiles in channel of height 500 nm (corresponds to the typical PillarHallTM case³).

Sticking coefficient c (-) is varied as: (a) 0.1 (b) 0.01 (c) 0.001. Exposure is constant at 10 Pa·s.

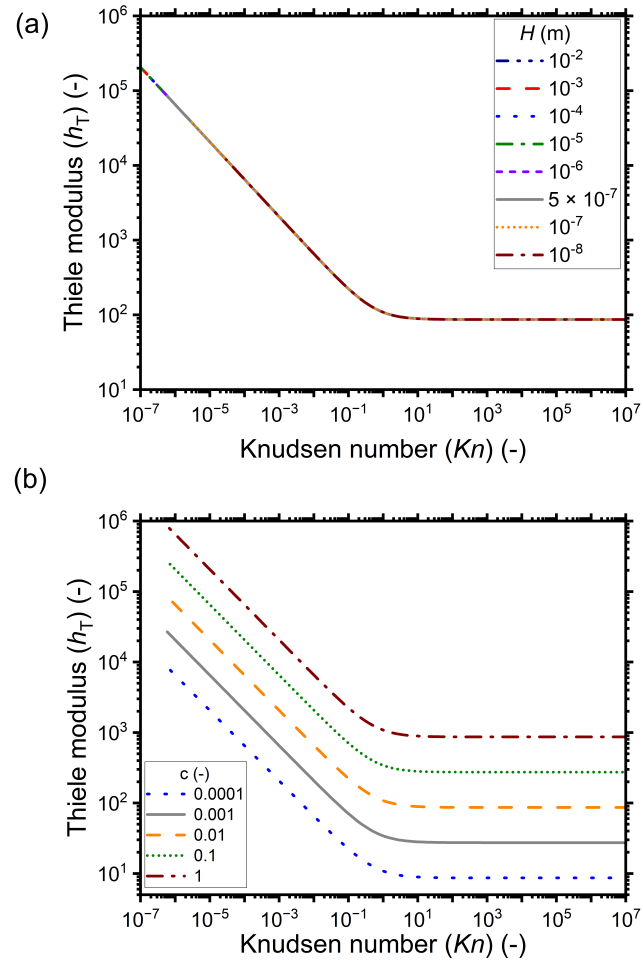


Figure S6 Thiele modulus plotted as a function of the Kn number for: (a) different channel heights with a sticking coefficient of 0.01, and (b) different sticking coefficients using a channel height of 500 nm (typical PillarHallTM case^{3,4}). The sticking coefficients have been varied as 1, 0.1, 0.01, 0.001 and 0.0001.

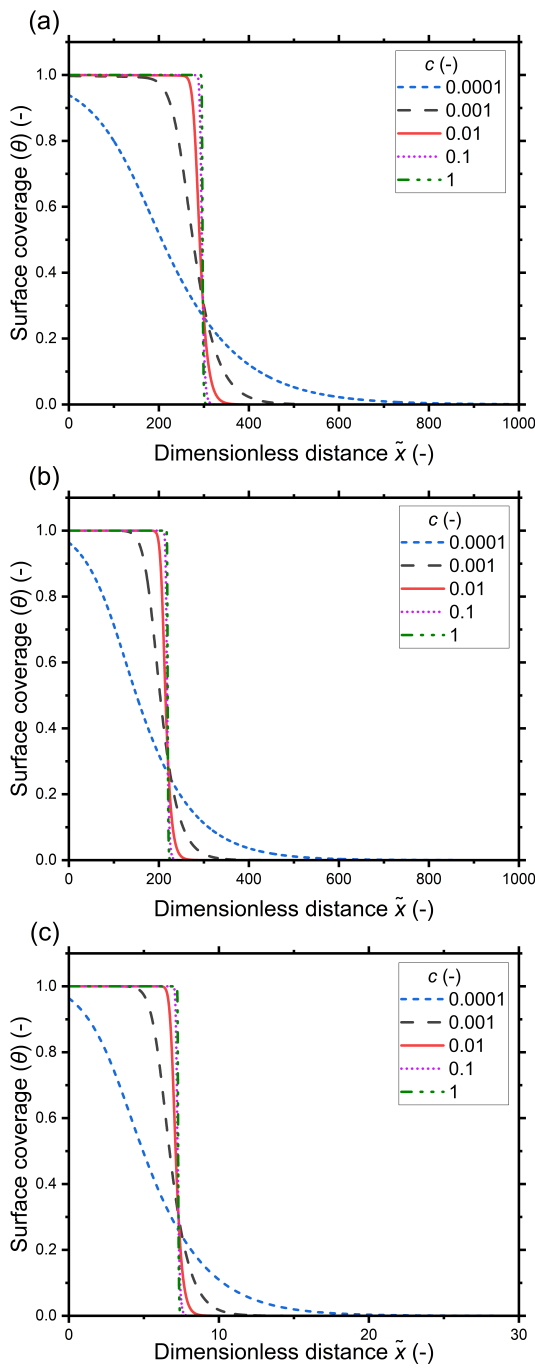


Figure S7 Saturation profiles with varying sticking coefficients for (a) free molecular flow regime, $Kn \sim 6 \times 10^4$ (b) transition regime, $Kn \sim 6 \times 10^{-1}$ and (c) continuum regime, $Kn \sim 3 \times 10^{-4}$. Note that the scale of the horizontal axis of panel (c) differs from the others.

Table S4 Simulation parameters varied for the summary table (Table 2) of the main article

	$\text{Kn} \gg 1$	$\text{Kn} \approx 1$	$\text{Kn} \ll 1$
Common center point parameters	$W = 10 \text{ mm}, N = 1, T = 573.15, t_1 = 0.1 \text{ s}, M_A = 0.1 \text{ kg mol}^{-1}, M_l = 0.028 \text{ kg mol}^{-1}, d_A = 6 \times 10^{-10} \text{ m}, d_l = 4 \times 10^{-10} \text{ m}, q = 4 \text{ nm}^{-2}, \rho = 3500 \text{ kg m}^{-3}, M = 0.05 \text{ kg mol}^{-1}, P_d = 0.01 \text{ s}^{-1}, c = 0.01$		
Additional center point parameters	$H = 5 \times 10^{-8} \text{ m}, p_{A0} = 50 \text{ Pa}, p_l = 250 \text{ Pa}$	$H = 5 \times 10^{-7} \text{ m}, p_{A0} = 500 \text{ Pa}, p_l = 2500 \text{ Pa}$	$H = 5 \times 10^{-4} \text{ m}, p_{A0} = 500 \text{ Pa}, p_l = 2500 \text{ Pa}$
Variied parameters	<p>Channel height H (m) $3 \times 10^{-8}, 4 \times 10^{-8}, 5 \times 10^{-8}, 6 \times 10^{-8}, 7 \times 10^{-8}$</p> <p>Initial partial pressure of the ALD reactant A p_{A0} (Pa) $1, 5, 10, 50, 100$</p> <p>Reactant pulse time t_1 (s) $0.001, 0.1, 1, 10, 100$</p> <p>Sticking coefficient c (-) $0.00001, 0.001, 0.01, 0.1, 1$</p> <p>Desorption probability P_d (s^{-1}) $0.001, 0.01, 0.1, 1, 10$</p> <p>Adsorption capacity q (nm^{-2}) $0.5, 1, 2, 4, 8$</p> <p>Temperature T (K) $373.15, 473.15, 573.15, 673.15, 773.15$</p> <p>Total pressure p (Pa) $50.5, 52, 60, 100, 300$</p> <p>Molar mass of the ALD reactant M_A (kg mol^{-1}) $0.05, 0.1, 0.15, 0.2, 0.25$</p> <p>Molar mass of the carrier gas M_l (kg mol^{-1}) $0.004, 0.012, 0.02, 0.028, 0.036$</p> <p>Size of the reactant molecule d_A (m) $4 \times 10^{-10}, 5 \times 10^{-10}, 6 \times 10^{-10}, 7 \times 10^{-10}, 8 \times 10^{-10}$</p> <p>Size of the carrier gas molecule d_l (m) $2 \times 10^{-10}, 3 \times 10^{-10}, 4 \times 10^{-10}, 5 \times 10^{-10}, 6 \times 10^{-10}$</p> <p>Density of the grown material ρ (kg m^{-3}) $2500, 3000, 3500, 4000, 4500$</p>	<p>$1.25 \times 10^{-7}, 2.5 \times 10^{-7}, 5 \times 10^{-7}, 1 \times 10^{-6}, 2 \times 10^{-6}$</p> <p>$100, 300, 500, 700, 1000$</p> <p>$0.001, 0.1, 1, 10, 100$</p> <p>$0.00001, 0.001, 0.01, 0.1, 1$</p> <p>$0.001, 0.01, 0.1, 1, 10$</p> <p>$0.5, 1, 2, 4, 8$</p> <p>$373.15, 473.15, 573.15, 673.15, 773.15$</p> <p>$1125, 1750, 3000, 5500, 10500$</p> <p>$0.05, 0.1, 0.15, 0.2, 0.25$</p> <p>$0.004, 0.012, 0.02, 0.028, 0.036$</p> <p>$4 \times 10^{-10}, 5 \times 10^{-10}, 6 \times 10^{-10}, 7 \times 10^{-10}, 8 \times 10^{-10}$</p> <p>$2 \times 10^{-10}, 3 \times 10^{-10}, 4 \times 10^{-10}, 5 \times 10^{-10}, 6 \times 10^{-10}$</p> <p>$2500, 3000, 3500, 4000, 4500$</p>	<p>$1 \times 10^{-4}, 2.5 \times 10^{-4}, 5 \times 10^{-4}, 7.5 \times 10^{-4}, 1 \times 10^{-3}$</p> <p>$100, 300, 500, 700, 1000$</p> <p>$0.00001, 0.001, 0.01, 0.1, 1$</p> <p>$0.00001, 0.001, 0.01, 0.1, 10$</p> <p>$0.5, 1, 2, 4, 8$</p> <p>$373.15, 473.15, 573.15, 673.15, 773.15$</p> <p>$1125, 1750, 3000, 5500, 10500$</p> <p>$0.05, 0.1, 0.15, 0.2, 0.25$</p> <p>$0.004, 0.012, 0.02, 0.028, 0.036$</p> <p>$4 \times 10^{-10}, 5 \times 10^{-10}, 6 \times 10^{-10}, 7 \times 10^{-10}, 8 \times 10^{-10}$</p> <p>$2 \times 10^{-10}, 3 \times 10^{-10}, 4 \times 10^{-10}, 5 \times 10^{-10}, 6 \times 10^{-10}$</p> <p>$2500, 3000, 3500, 4000, 4500$</p>

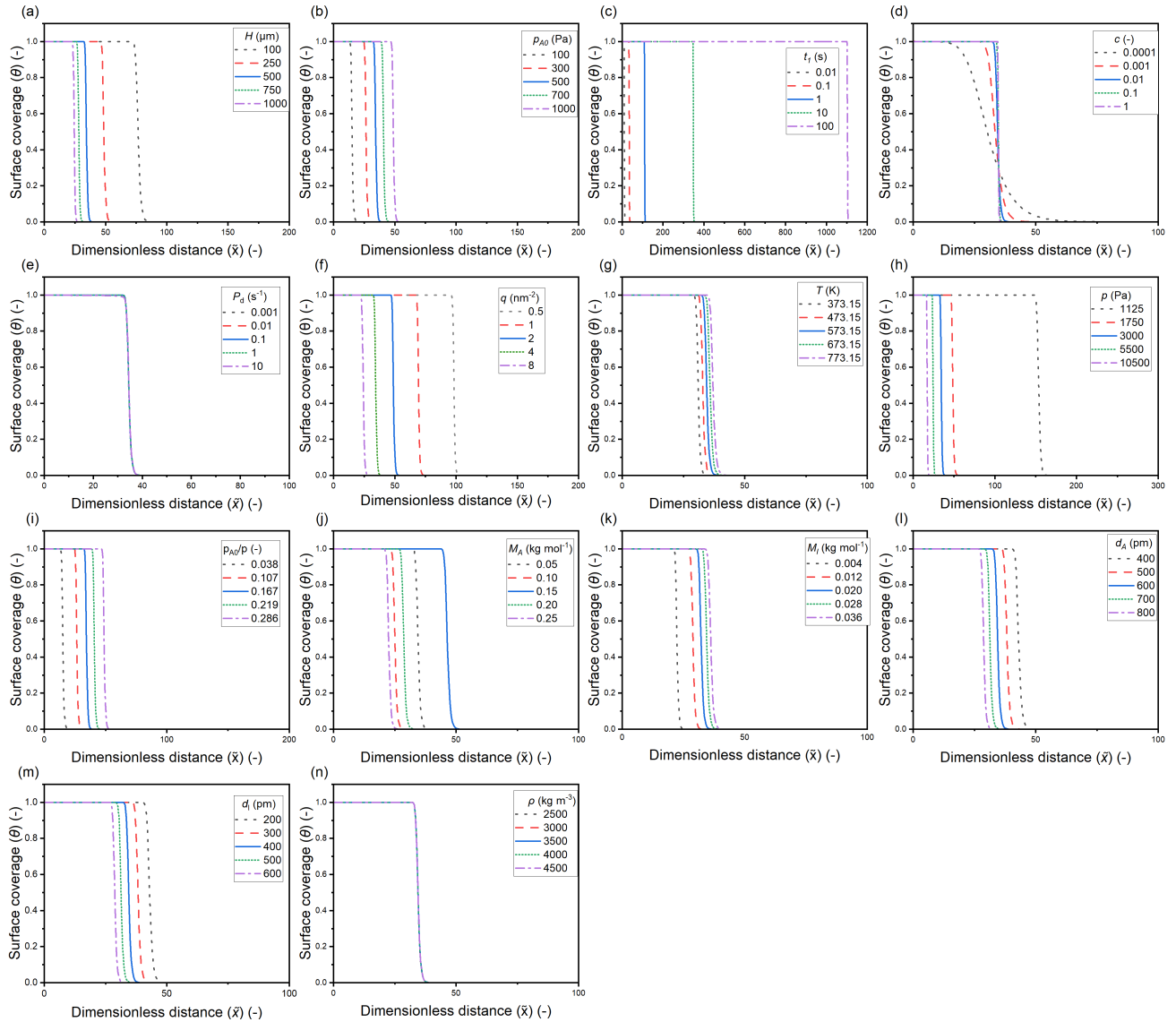


Figure S8 Saturation profiles corresponding to the summary table of the main article (Table 2), simulated in the continuum flow regime ($Kn \ll 1$), by implementing Yililammi *et al.*⁵ model with varying (a) channel height H , (b) initial partial pressure of reactant A p_{A0} , (c) pulse length t , (d) sticking coefficient c , (e) desorption probability P_d , (f) adsorption density q , (g) temperature T , (h) total pressure p , (i) ratio between initial partial pressure of reactant A to total pressure p_{A0}/p , (j) molar mass of reactant A M_A , (K) molar mass of inert gas M_I , (l) diameter of reactant A d_A , (m) diameter of inert gas d_I , and (n) film density ρ . Saturation profiles for the transition and free molecular flow regime are in a previous work by Yim *et al.*¹

Table S5 Penetration depth and absolute values of the slope at half coverage for the summary table (Table 2) of the main article. The values are for trends reported in the continuum regime ($Kn \ll 1$).

Simulation parameter	Varied values	$\tilde{x}_{\theta=0.5}$	$\left \frac{d\theta}{d\tilde{x}} \right _{\tilde{x}=0.5}$
Channel height H (μm)	100	76.527	0.229
	250	48.630	0.363
	500	34.433	0.518
	750	28.121	0.641
	1000	24.354	0.748
Initial partial pressure of the ALD reactant A p_{A0} (Pa)	100	15.159	0.531
	300	26.575	0.524
	500	34.433	0.518
	700	40.818	0.512
	1000	48.867	0.504
Reactant pulse time t_1 (s)	0.01	10.572	0.519
	0.1	34.433	0.518
	1	109.887	0.518
	10	348.494	0.518
	100	1103.037	0.517
Sticking coefficient c (-)	0.0001	30.196	0.052
	0.001	33.432	0.164
	0.01	34.432	0.518
	0.1	34.749	1.638
	1	34.849	5.179
Desorption probability P_d (s^{-1})	0.0001	34.432	0.518
	0.001	34.432	0.518
	0.01	34.433	0.518
	0.1	34.433	0.518
	1	34.441	0.518
Adsorption density q (nm^{-2})	0.5	98.235	0.519
	1	69.326	0.519
	2	48.885	0.517
	4	34.431	0.517
	8	24.211	0.518
Temperature T (°C)	373.15	30.991	0.642
	473.15	32.852	0.570
	573.15	34.433	0.518
	673.15	35.814	0.478
	773.15	37.047	0.447
Total pressure p (Pa)	1125	153.662	0.184
	1750	48.579	0.355
	3000	34.431	0.517
	5500	24.375	0.739
	10500	17.246	1.053
Fraction of reactant pressure of total pressure p_{A0}/p (-)	0.038	15.159	0.530
	0.107	26.574	0.524
	0.167	34.431	0.519
	0.219	40.816	0.512
	0.286	48.864	0.502

Simulation parameter	Varied values	$\tilde{x}_{\theta=0.5}$	$\left \frac{d\theta}{d\tilde{x}} \right _{\tilde{x}=0.5}$
Molecular mass of the ALD reactant M_A (kgmol $^{-1}$)	0.05	46.416	0.455
	0.1	34.433	0.518
	0.15	28.621	0.565
	0.2	25.014	0.603
	0.25	22.497	0.635
Molecular mass of the carrier gas M_I (kgmol $^{-1}$)	0.004	22.327	0.813
	0.012	28.825	0.625
	0.02	32.179	0.557
	0.028	34.432	0.518
	0.036	36.105	0.493
Size of the reactant molecule d_A (m)	4	43.005	0.420
	5	38.245	0.468
	6	34.431	0.516
	7	31.308	0.568
	8	28.704	0.614
Density of the grown material ρ (kgm $^{-3}$)	2000	34.433	0.518
	2500	34.433	0.518
	3000	34.432	0.518
	3500	34.432	0.518
	4000	34.433	0.518

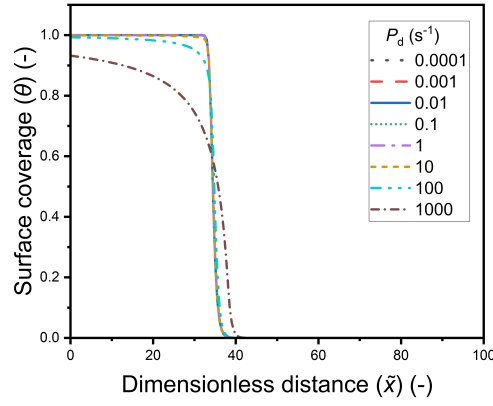


Figure S9 Saturation profiles with increasing the desorption probability P_d in the continuum flow regime used in the summary table of the main article (Table 2). This figure also includes additional saturation profiles for higher P_d values ($P_d \geq 10$).

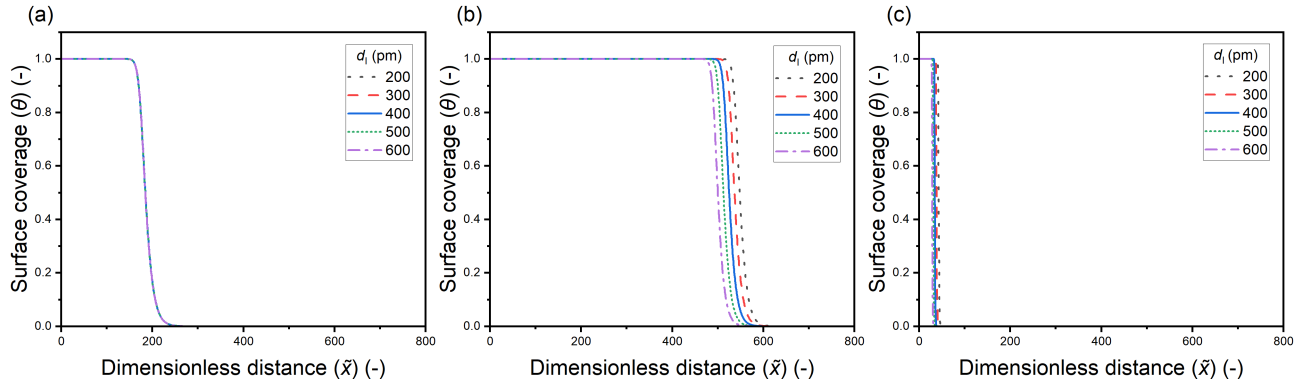


Figure S10 Saturation profiles for increasing the diameter of the inert carrier gas d_l related to the summary table in the main article (Table 2). The saturation profiles are for different flow regimes: (a) free molecular flow regime (b) transition flow regime and the (c) continuum flow regime.

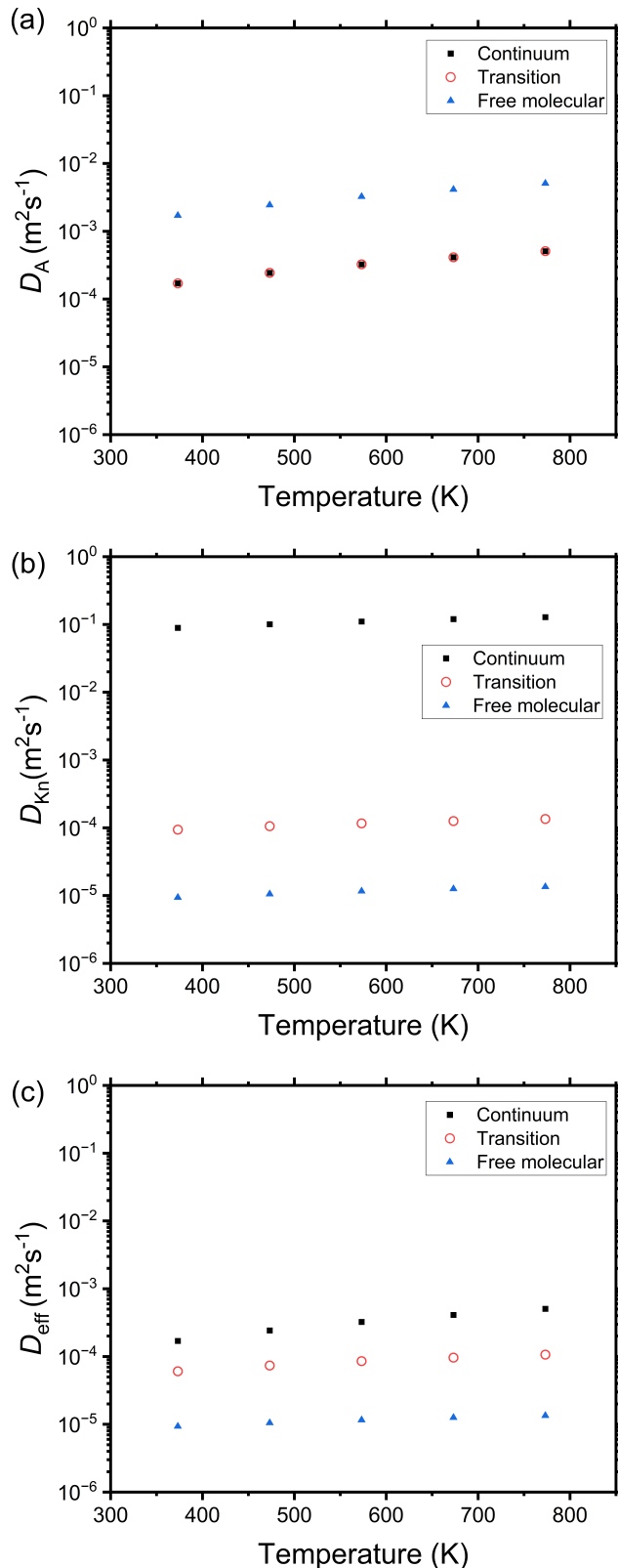


Figure S11 Diffusion coefficients ($\text{m}^2 \text{s}^{-1}$) corresponding to the temperature T variation cases in the summary Table 2 of the main article. Diffusion coefficients are plotted as a function of T (K): (a) molecular diffusion coefficient D_A , (b) Knudsen diffusion coefficient D_{Kn} , and (c) effective diffusion coefficient D_{eff} .

References

- [1] J. Yim, E. Verkama, J. A. Velasco, K. Arts and R. L. Puurunen, *Physical Chemistry Chemical Physics*, 2022, **24**, 8645–8660.
- [2] R. G. Gordon, D. Hausmann, E. Kim and J. Shepard, *Chemical Vapor Deposition*, 2003, **9**, 73–78.
- [3] PillarHall® – Lateral High Aspect Ratio Test Structures, Accessed May 12, 2023, <http://pillarhall.com/>.
- [4] J. Yim, O. M. Ylivaara, M. Ylilammi, V. Korpelainen, E. Haimi, E. Verkama, M. Utriainen and R. L. Puurunen, *Physical Chemistry Chemical Physics*, 2020, **22**, 23107–23120.
- [5] M. Ylilammi, O. M. Ylivaara and R. L. Puurunen, *Journal of Applied Physics*, 2018, **123**, 205301.